Supplementary information

Sunlight-activated Eu^{3+}-doped $CaNaSb_2O_6F$ yellow-orange long persistent luminescence material

Xuexia Chen,[a,b] Ran Pang, [a,*] Shangwei Wang,[a] Weihong Yuan, [a,b] Jiangyue Su, [a,b] Tao Tan, [a,b] Su Zhang, [a,*] Chengyu Li, [a,b] and Hongjie Zhang [a]

a State Key Laboratory of Rare Earth Resource Utilization, Changchun Institute of Applied Chemistry, Chinese Academy of Sciences, Changchun 130022, P. R. China.

b School of Applied Chemistry and Engineering, University of Science and Technology of China, Hefei 230026, P. R. China

** Corresponding author: Tel: +86-0431-85262258*

E-mail address: pangran@ciac.ac.cn

Tables and Table Captions

Table S1. Structure Refinement Parameters of CNSOF and CNSOF:0.05Eu^{3+} samples.

Formula		CNSOF			
Space group		Cubic, *Fd*-3*m*（277）			
Cell parameters		a = 10.2850（1） Å, V = 1087.97（2） $Å^3$, Z = 8			
R_{wp}, R_p, χ^2		R_{wp} = 8.08%, R_p =5.47%, χ^2 = 9.52			
Atom	Wyck	x	y	z	Occpancy
Na1	16d	0.625	0.625	0.625	0.5
Ca1	16d	0.625	0.625	0.625	0.5
Sb1	16c	0.125	0.125	0.125	1
O1	48f	0.2	0	0	1
F1	8b	0.5	0.5	0.5	1
Formula		CNSOF：0.05Eu^{3+}			
Space group		Cubic, *Fd*-3*m*（277）			
Cell parameters		a = 10.3096（1） Å, V = 1095.77（2） $Å^3$, Z = 8			
R_{wp}, R_p, χ^2		R_{wp} = 6.41%, R_p = 4.24%, CHI^2 = 6.258			
Atom	Wyck	x	y	z	Occpancy
Na1	16d	0.625	0.625	0.625	0.5
Ca1	16d	0.625	0.625	0.625	0.475
Sb1	16c	0.125	0.125	0.125	1
O1	48f	0.2	0	0	1
F1	8b	0.5	0.5	0.5	1
Eu1	16d	0.625	0.625	0.625	0.025

The radius percentage difference (D_R) of Eu^{3+} and cationic sites is estimated according to the following equation reported by Davolos:[1]

$$D_r = \frac{|R_m(CN) - R_d(CN)|}{R_m(CN)} \times 100\% \quad (1)$$

where *CN* is the coordination number of ions, and R_m (*CN*) and R_d (*CN*) represent the radius of host cations and doped ions, respectively. In this work, the calculated D_r values of Eu^{3+} occupying host cationic sites of Na^+, Ca^{2+} and Sb^{5+} are about 5.93%, 11.61% and 95.00%, respectively.[2] Obviously, the Sb^{5+} sites are too small and the charge difference is large, so that Eu^{3+} ion can hardly occupy the Sb^{5+} site. Combined with the law of XRD peak position shift, it is further indicated that Eu^{3+} ions take the Na^+ or Ca^{2+} sites with smaller radius, accompanied by the expansion of the main lattice volume.

Table S2. Bond details of Na/Ca-O/F in the CNSOF.

Bond	Length(Å)	Bonds	Angle(degree)
Na1-O1^{I}	2.5613	O1^{I}-Na1-O1^{II}	117.0357
Na1-O1^{II}	2.5613	O1^{I}-Na1-O1^{III}	117.0357
Na1-O1^{III}	2.5613	O1^{I}-Na1-O1^{IV}	180
Na1-O1^{IV}	2.5613	O1^{I}-Na1-O1^{V}	62.9643
Na1-O1^{V}	2.5613	O1^{I}-Na1-O1^{VI}	62.9643
Na1-O1^{VI}	2.5613	O1^{I}-Na1-F1^{I}	79.975
Na1-F1^{I}	2.2293	O1^{I}-Na1-F1^{II}	100.025
Na1-F1^{II}	2.2293		
Ca1-O1^{I}	2.5613	O1^{I}-Ca1-O1^{II}	117.0357
Ca1-O1^{II}	2.5613	O1^{I}-Ca1-O1^{III}	117.0357
Ca1-O1^{III}	2.5613	O1^{I}-Ca1-O1^{IV}	180
Ca1-O1^{IV}	2.5613	O1^{I}-Ca1-O1^{V}	62.9643
Ca1-O1^{V}	2.5613	O1^{I}-Ca1-O1^{VI}	62.9643
Ca1-O1^{VI}	2.5613	O1^{I}-Ca1-F1^{I}	79.975
Ca1-F1^{I}	2.2293	O1^{I}-Ca1-F1^{II}	100.025
Ca1-F1^{II}	2.2293		

According to the refined data, the lattice distortion *D* of the crystal Ca/Na co-occupying site is analyzed and calculated by the following formula:[3]

$$D = \frac{1}{n}\sum_{i=1}^{n}\frac{|l_i - l_{av}|}{l_{av}} \quad (2)$$

where l_i refers to the distance between the ith coordination atom and the central atom,

l_{av} represents the average bond length, and n is the coordination number. Based on the refined data, the bond length distortion index of the Ca/NaO_6F_2 dodecahedron is calculated to be 0.05. The angle between the opposite O atoms or F atoms is 180 °, and Ca/Na is in the symmetry center of dodecahedron.

Figures and Figure Captions

(a)

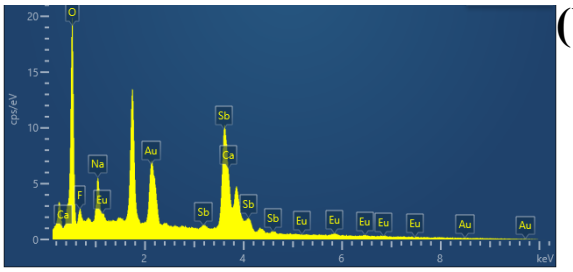

(b)

Element	Wt%	Wt% Sigma	At%
O	20.78	0.56	54.23
F	3.68	0.41	8.10
Na	4.60	0.26	8.37
Ca	7.71	0.39	8.04
Sb	57.14	1.41	19.60
Eu	6.08	2.13	1.67
Total	100.00		100.00

Figure S1. (a) EDS analysis spectrum of the $CaNaSb_2O_6F$:0.05Eu^{3+} phosphor. (b) Content of different elements.

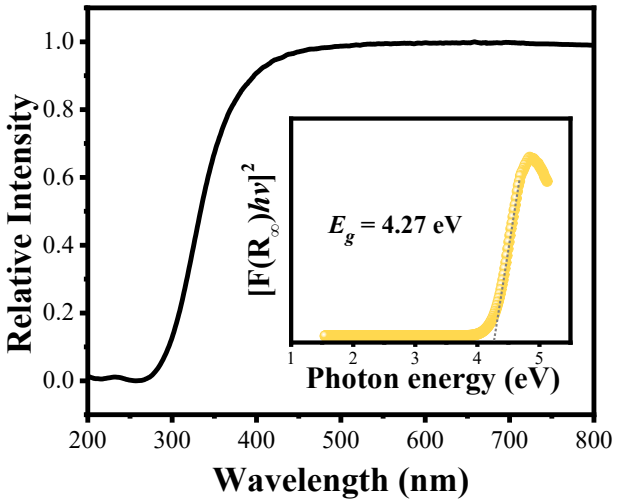

Figure S2. DRS of CNSOF host; the inset presents the calculated optical bandgap values.

The optical band gap value (E_g) of CNSOF can be calculated according to the following formula:[4,5]

$$F(R) = \frac{(1-R)^2}{2R} \tag{3}$$

$$[F(R)hv]^n = D(hv - E_g) \tag{4}$$

where R represents the reflection parameter (%), $F(R)$ represents the absorption coefficient, D denotes the absorption constant, and hv refers to the corresponding photon energy (eV). Meanwhile, the value of n depends on the type of band gap: $n = 2$ is used for direct band gap, and $n = 1/2$ is used for indirect band gap. The calculation results of the band structure show that CNSOF sample belongs to direct band gap (n = 2). According to the DRS spectrum of the sample, the optical band gap E_g value of CNSOF is calculated to be about 4.27 eV by extrapolating to $[F(R)hv]^2 = 0$, as exhibited in the inset of Figure S2.

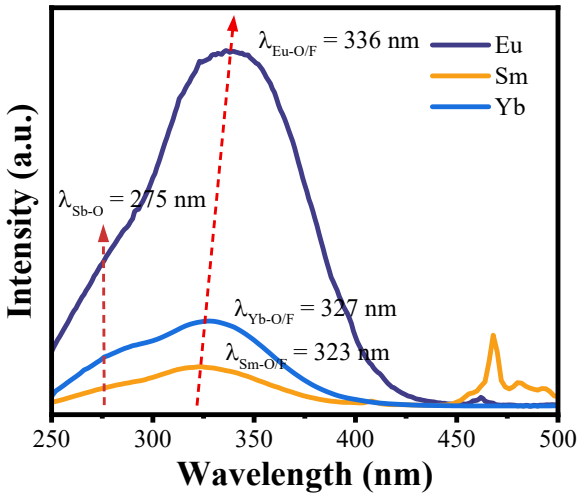

Figure S3. The PLE spectra of CNSOF:0.05Eu^{3+}(λ_{em} = 641 nm), CNSOF:0.05 Sm^{3+}(λ_{em} = 612 nm) and CNSOF:0.05 Yb^{3+}(λ_{em} = 974 nm).

The CTB presents in many Sm^{3+}, Eu^{3+}, Yb^{3+}-doped phosphors. In the same host, the relationship between the charge transfer energy of rare earth ions and Eu^{3+} is as follows:[5, 6]

$$E^{CT}(n,3+,A) = E_{CT}(6,3+,A) + \Delta E^{CT}(n,6,3+)$$

where, E^{CT} (n,3+,A) is the charge transfer energy of trivalent rare earth ions with n electrons in 4f layer in host A, and ΔE^{CT} (n,6,3+) is the difference of charge transfer energy between some trivalent rare earth ions and Eu^{3+} ions. According to the statistical results, the value of ΔE^{CT} (n,6,3+) varies with different rare earth ions, and the order is Er^{3+} > Dy^{3+} > Tm^{3+} > Sm^{3+} > Yb^{3+} > Eu^{3+}.[7, 8] The PLE spectra of CNSOF:0.05Eu^{3+}(λ_{em} = 641 nm), CNSOF:0.05 Sm^{3+} (λ_{em} = 612 nm) and CNSOF:0.05 Yb^{3+} (λ_{em} = 974 nm) were measured, and the charge transfer of O^{2-}-Sb^{5+} at 275 nm was observed in all the samples. The charge transfer energy is Sm^{3+} > Yb^{3+} > Eu^{3+}, which further confirms the existence of the CTB.

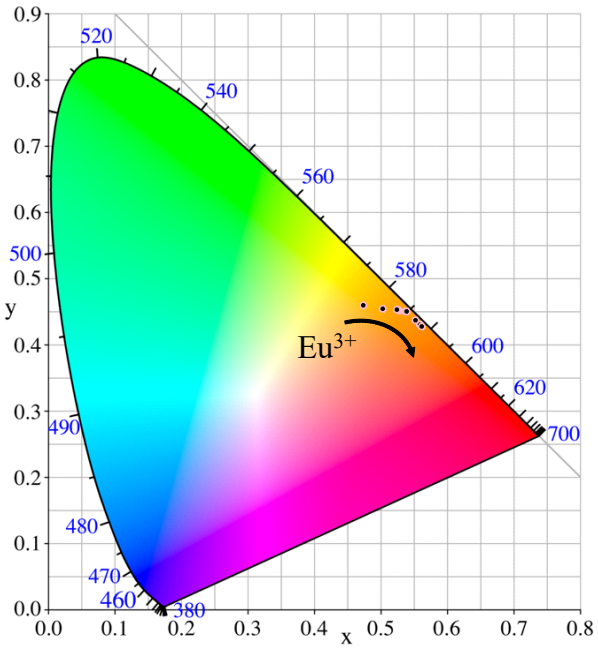

Figure S4. CIE (*x*, *y*) coordinate diagram of CNSOF:*x*Eu^{3+}(0.01≤*x*≤0.08) phosphors **under 336 nm excitation**.

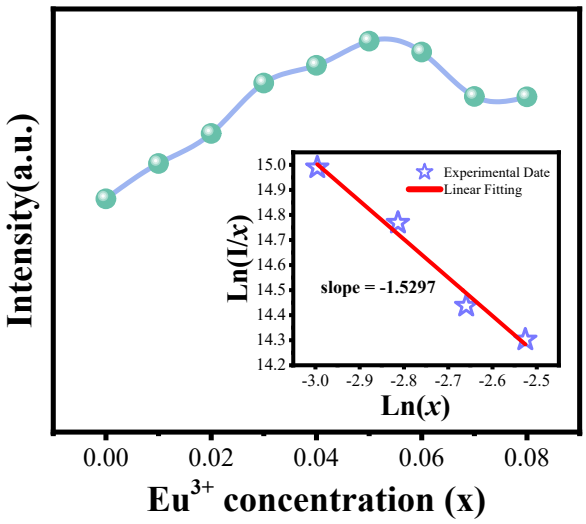

Figure S5. The dependence of the emission intensity on content of Eu^{3+} ion doping concentration; the inset shows The relationship between Ln(I/x) and Ln(x) for CNSOF:$x$$Eu^{3+}$ ($0.05 \leq x \leq 0.08$) .

The critical distance (R_c) of energy transfer among Eu^{3+} ions can be further identified by estimating the following expression:[9]

$$R_c = 2 \times \left[\frac{3V}{4\pi x_c Z}\right]^{\frac{1}{3}} \quad (5)$$

where V is the volume of the unit cell, x_c represents the optimal concentration of activator ions, and Z refers to the number of cation sites suitable for doping in each unit cell. For CNSOF:$x$$Eu^{3+}$ ($0 \leq x \leq 0.08$), V = 1087.97 Å^3, Z = 8, and the critical concentration of Eu^{3+} is x_c = 0.05. Therefore, the average distance of the R_c is estimated to be about 17.32 Å. Generally, multipole interaction and exchange interaction are two types of energy transfer mechanisms. When R_c is less than or about 5 Å, it belongs to exchange interaction.[10] At this time, the R_c is much larger than 5 Å, proving again that the concentration quenching should be mainly dominated by multipole interaction

mechanism.

According to Dexter theory, the multipole interaction mechanism of energy transfer can be determined by using the following expression:[11]

$$\frac{I}{x} = \frac{K}{\left[1 + \beta\,(x)^{\frac{\theta}{3}}\right]} \tag{6}$$

here, I is the integrated emission intensity, x is the concentration of the activator ion, K and β are the constants for the given host lattice under the same excitation conditions, and θ= 6, 8 and 10 denote dipole-dipole (d-d), dipole-quadrupole (d-q) and quadrupole-quadrupole (q-q) interactions, respectively. The inset of Figure S5 displays the functional relationship between Ln(I/x) and Ln(x) of CNSOF:xEu^{3+} ($0.05 \leq x \leq 0.08$). By linear fitting, the correlation coefficient is 1.5297. Therefore, the value of θ can be estimated to be 4.5891, which is closest to 6, manifesting that the most likely concentration quenching mechanism of Eu^{3+} in CNSOF:xEu^{3+} phosphors should be dipole-dipole interaction.

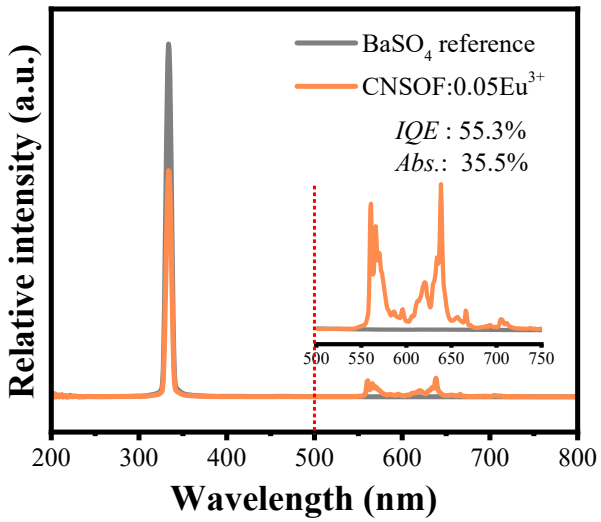

Figure S6. The quantum efficiencies of the CNSOF:0.05Eu^{3+} phosphor.

The absorption efficiency (ξ_{abs}), internal quantum efficiency (*IQE*) and external quantum efficiency (*EQE*) were calculated respectively by the following equation:[12, 13]

$$\xi_{abs} = \frac{\int E_R - \int E_S}{\int E_R} \tag{7}$$

$$IQE = \frac{\int L_S}{\int E_R - \int E_S} \tag{8}$$

$$EQE = IQE \times \xi_{abs} \tag{9}$$

here, $\int L_S$ stands for the integral area of the emission spectra, and $\int E_S$ and $\int E_R$ represent the integral area of the excitation spectrum with and without phosphors in the integrating sphere, respectively. As shown in Figure S6, under 336 nm excitation, the wavelength of the emission peak is basically the same as that of Figure 4a, but the peak intensity is different.[14] This divergence is caused by resolutions of different instruments. The values of *IQE*, ξ_{abs} and *EQE* of yellow-orange phosphor CNSOF:0.05Eu^{3+} are calculated to be 55.3%, 35.5% and 19.6%, respectively.

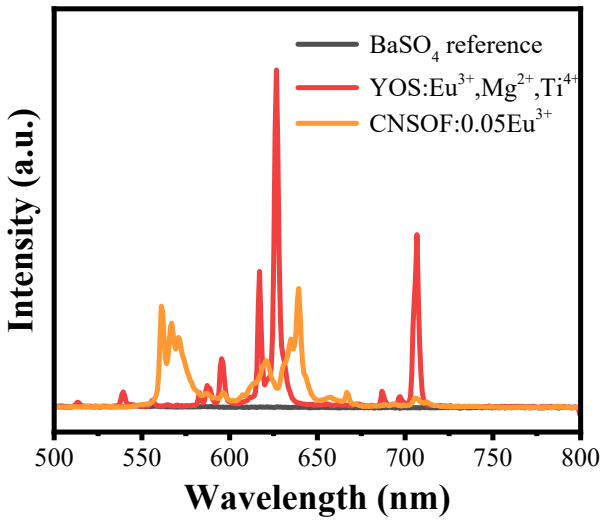

Figure S7. Emission spectra of $Y_2O_2S:Eu^{3+}$, Mg^{2+}, Ti^{4+}, $CNSOF:Eu^{3+}$ phosphor and reference samples recorded by a spectrofluorometer equipped with an integrating sphere for QE measurement.

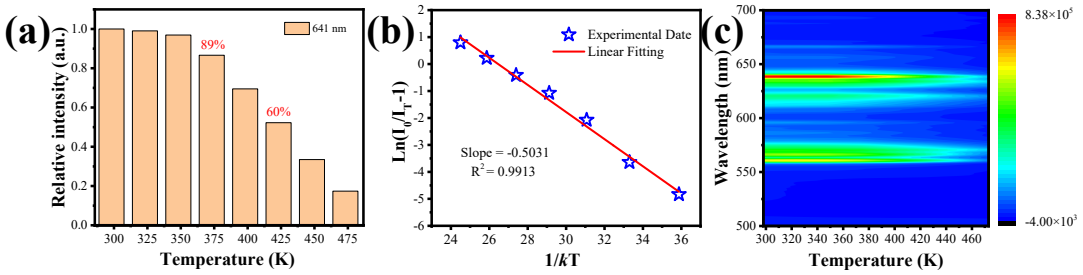

Figure S8. (a) **Integrated emission intensity measured at different temperature**. (b) The plots fitted activation energy for thermal quenching. (c)Temperature-dependent emission spectra (λ_{ex} = 334 nm) **of** CNSOF:0.05Eu^{3+}.

Using the PL intensity of I_0 and I_T at different temperatures T, the thermal activation energy barrier (E_a) can be obtained by Arrhenius equation:[15]

$$\frac{I_T}{I_0} = [1 + Dexp\left(\frac{-E_a}{kT}\right)]^{-1} \quad (10)$$

where T, I_T, I_0, D, E_a and k represent the working temperature, the PL intensity at T, the PL intensity at 298 K, the constant, the activation energy and the Boltzmann constant, respectively. The curve between ln[(I_0/I_T)−1] and 1/kT is shown in Figure S8b, and the E_a value corresponding to the linearly fitted slope is 0.5031 eV.

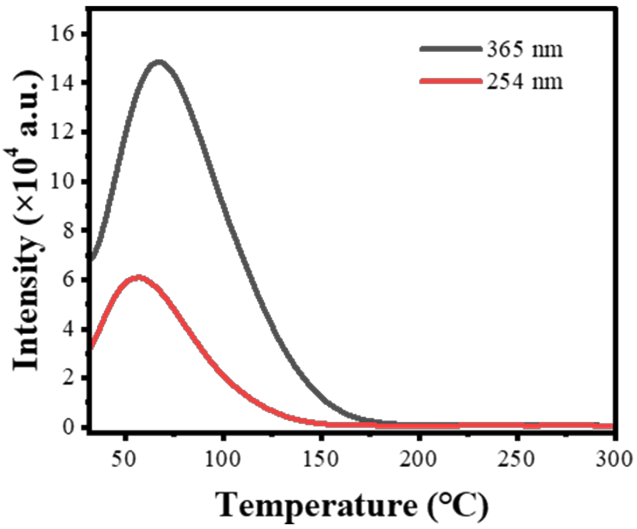

Figure S9. TL curves **of CNSOF:0.05Eu^{3+} phosphor under** at 254 nm and 365nm **excitation**, respectively.

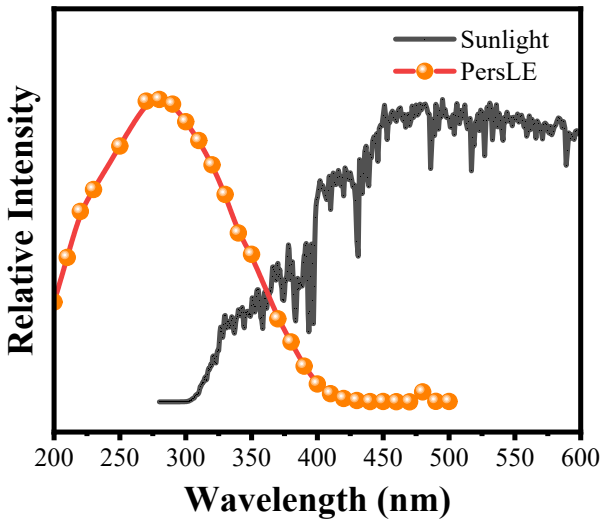

Figure S10. Normalized PersLE spectra of CNSOF:0.05Eu^{3+} phosphor and the solar spectrum received at the Earth's surface.

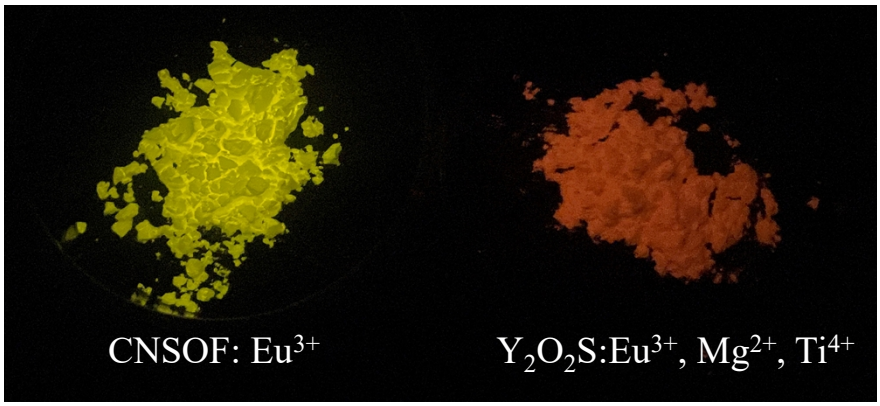

Figure S11. Photograph of the initial PersL of the prepared **CNSOF: Eu^{3+} sample** and **Y_2O_2S: Eu^{3+}, Mg^{2+}, Ti^{4+} phosphor**.

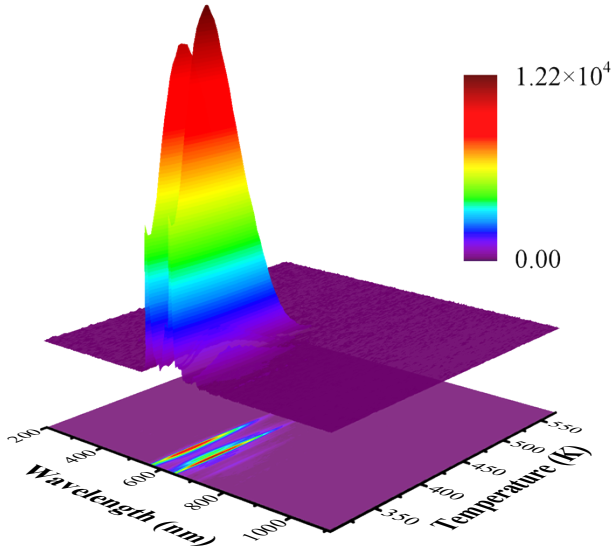

Figure S12. 3D-TL curves **of** CNSOF:0.05Eu^{3+} phosphor.

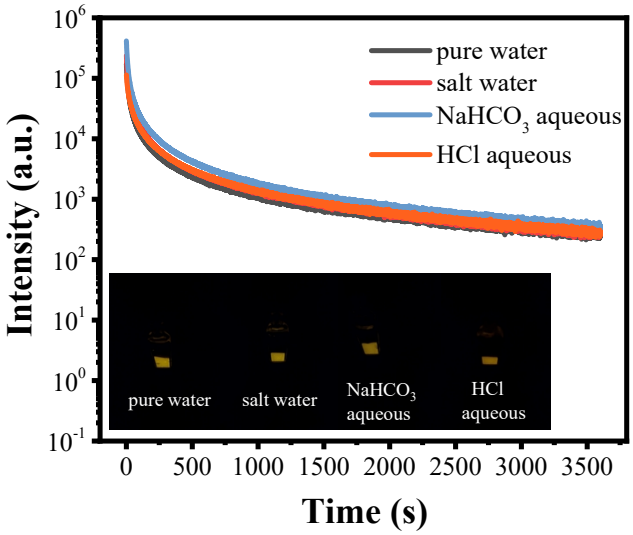

Figure S13. After being irradiated by direct sunlight for 10 min, the PersL decay curves of CNSOF:0.05Eu^{3+} phosphors **recorded at** different surrounding media, and the insets show the corresponding PersL photographs of the samples.

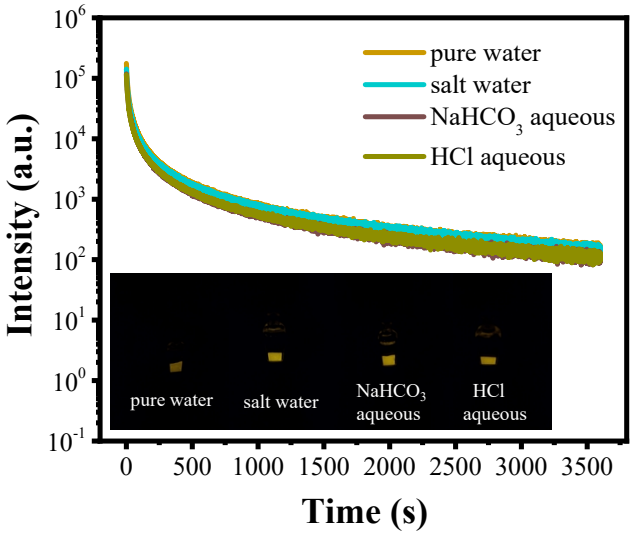

Figure S14. After being irradiated by direct sunlight for 10 min, the PersL decay curves of CNSOF:0.05Eu^{3+} phosphors **recorded at** different surrounding media for three days, and the insets show the corresponding PersL photographs of the samples.

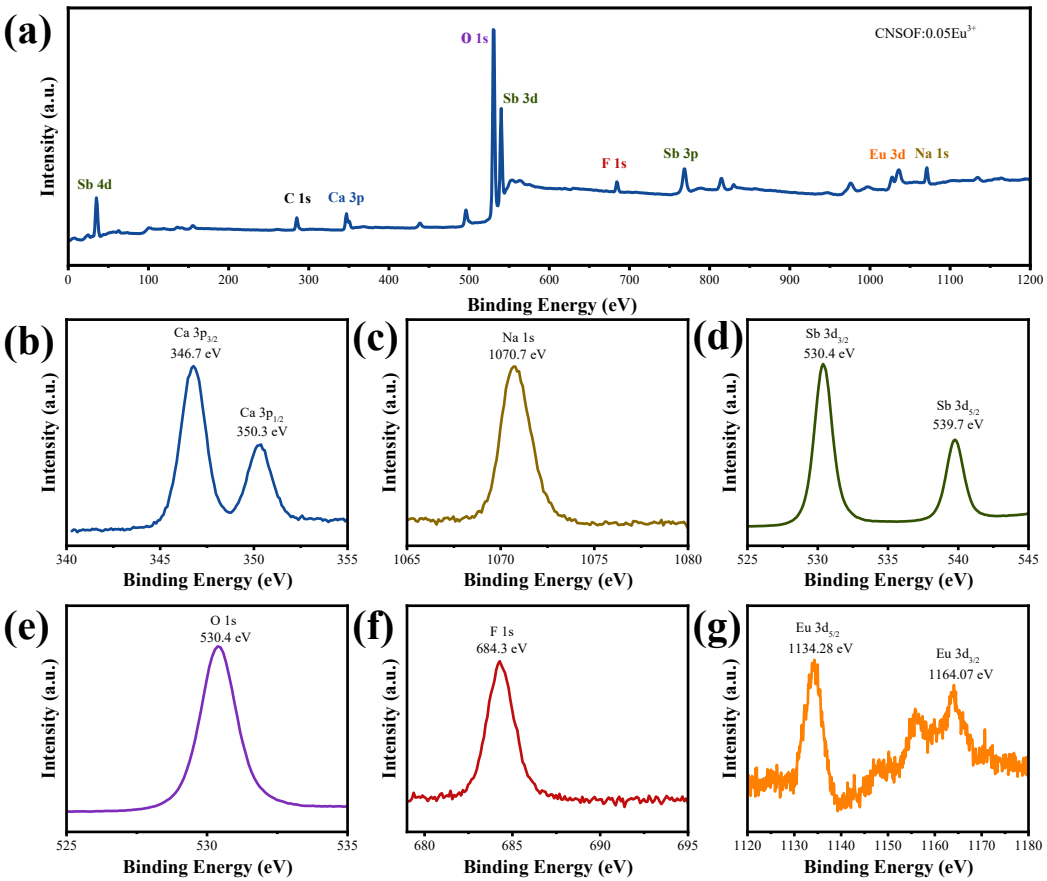

Figure S15. (a) XPS and (b-g) HR XPS spectra of the representative CNSOF:0.05Eu^{3+} phosphor.

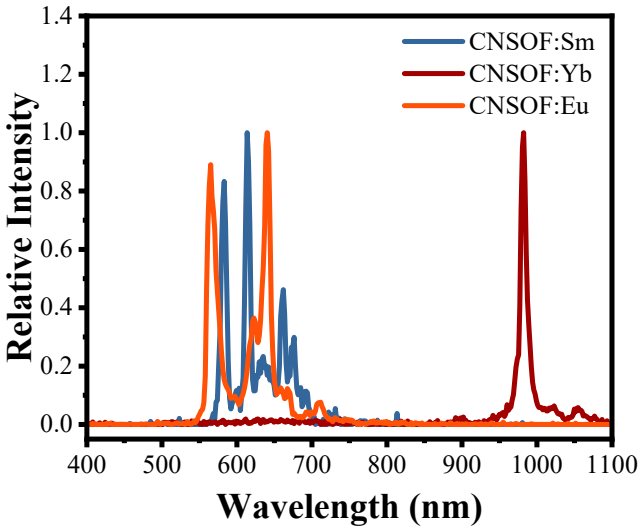

Figure S16. The PersL spectra of CNSOF:0.05Eu^{3+}, CNSOF:0.05Sm^{3+} and CNSOF:0.05Yb^{3+}.

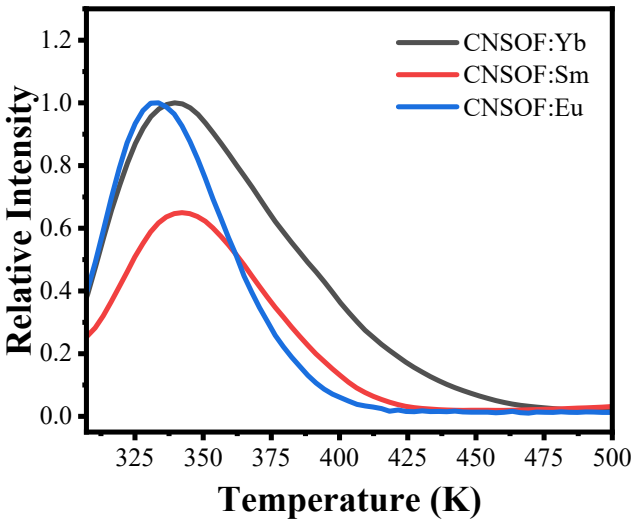

Figure S17. The TL curves of CNSOF doped with Sm^{3+}, Yb^{3+} and Eu^{3+}.

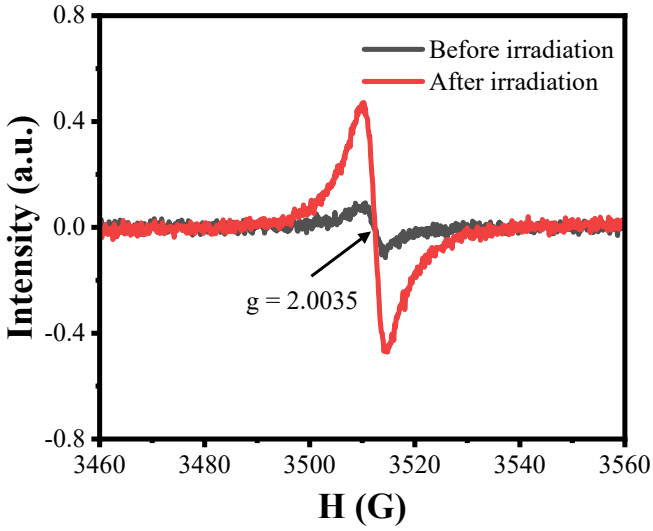

Figure S18 EPR spectra of CNSOF:Eu^{3+} measured before and after illumination by a 365 nm UV lamp.

Supplementary References

1 A. M. Pires, M. R. Davolos, Luminescence of Europium(III) and Manganese(II) in Barium and Zinc Orthosilicate, *Chem. Mater.*, 2001, **13**, 21-27.

2 X. Chen, R. Pang, S. Wang, J. Su, W. Yuan, S. Jiao, H. Wu, D. Li, C. Li, H. Zhang, Design and synthesis of a novel blue-emitting $CaNaSb_2O_6F:Bi^{3+}$ phosphor for optical temperature sensing, *Dalton Trans.*, 2022, **51**, 6908-6917.

3 S. Wang, H. Wu, Y. Fan, Q. Wang, T. Tan, R. Pang, S. Zhang, D. Li, L. Jiang, C. Li, H. Zhang, A highly efficient narrow-band blue phosphor of Bi^{3+}-activated cubic borate $Ba_3Lu_2B_6O_{15}$ towards backlight display applications, *Chem. Eng. J.*, 2022, **432**, 134265.

4 A. E. Morales, E. S. Mora, U. Pal, Use of diffuse reflectance spectroscopy for optical characterization of un-supported nanostructures, *Rev. Mex. Fís.*, 2007, **53**, 18-22.

5 G. Cao, L. Rabenberg, C. M. Nunn, T. E. Mallouk, Formation of quantum-size semiconductor particles in a layered metal phosphonate host lattice, *Chem. Mater.*, 1991, **3**, 149-156.

6 E. Radzhabov, Creation of trapped electrons and holes in alkaline-earth fluoride crystals doped by rare-earth ions, *J. Phys. Condens. Matter*, 2001, **13**, 10955.

7 P. Dorenbos, Systematic behaviour in trivalent lanthanide charge transfer energies, *J. Phys. Condens. Matter*, 2003, **15**, 8417.

8 U. Happek, S. A. Basun, J. Choi, J. K. Krebs, M. Raukas, Electron transfer processes in rare earth doped insulators, *J. Alloys Compd.*, 2000, **303-304**, 198-206.

9 G. Blasse, A. Bril, Investigations on Bi^{3+}-activated phosphors, *J. Chem. Phys.*, 1968, **48**, 217-222.

10 Q. Wu, Y. Li, Y. Wang, H. Liu, S. Ye, L. Zhao, J. Ding, J. Zhou, A novel narrow-band blue-emitting phosphor of Bi^{3+}-activated $Sr_3Lu_2Ge_3O_{12}$ based on a highly symmetrical crystal structure used for WLEDs and FEDs, *Chem. Eng. J.*, 2020, **401**, 126130.

11 L. G. Van Uitert, Characterization of Energy Transfer Interactions between Rare Earth Ions, *J. Electrochem. Soc.*, 1967, **114**, 1048.

12 S. Leyre, E. Coutino-Gonzalez, J. J. Joos, J. Ryckaert, Y. Meuret, D. Poelman, P. F. Smet, G. Durinck, J. Hofkens, G. Deconinck, P. Hanselaer, Absolute determination of photoluminescence quantum efficiency using an integrating sphere setup, *Rev. Sci. Instrum.*, 2014, **85**, 123115.

13 Q. Dong P. Xiong, J. Yang, Y. Fu, W. Chen, F. Yang, Z. Ma, M. Peng, Bismuth activated blue phosphor with high absorption efficiency for white LEDs, *J. Alloys Compd.*, 2021, **885**, 160960.

14 M. Wu, B. Chen, C. He, X. Huang, Q. Liu, X. Min, R. Mi, X. Wu, M. Fang, Y. G. Liu, Z. Huang, A high quantum yield red phosphor $NaGdSiO_4$: Eu^{3+} with intense

emissions from the $^5D_0 \rightarrow {}^7F_{1,2}$ transition, *Ceram. Int.*, 2022, **48**, 23213-23223.

15 J. Wang, M. Zhang, Q. Zhang, W. Ding, Q. Su, The photoluminescence and thermoluminescence properties of novel green long-lasting phosphorescence materials $Ca_8Mg(SiO_4)_4Cl_2:Eu^{2+},Nd^{3+}$, *Appl. Phys. B.*, 2007, **87**, 249-254.